BMC Cancer

RESEARCH Open Access

FTO-mediated demethylation of MTUS1/ATIP1 promotes tumor progression in head and neck squamous cell carcinoma

Dongxiao Tang[1,2†], Congyuan Cao[1†], Wuguo Li[3] and Anxun Wang[1*]

Abstract

Background Head and neck squamous cell carcinoma (HNSCC) has been recognized as the seventh most prevalent malignant tumor globally. It is a malignant neoplasm that arises from the mucosal epithelium of head and neck region. In our previous research, we have demonstrated that MTUS1/ATIP1 exhibits anti-cancer properties in HNSCC. Nevertheless, the underlying mechanism responsible for the reduction of MTUS1/ATIP1 expression has not been investigated.

Methods HNSCC and adjacent normal tissues were collected and examined using m^{6}A MeRIP-seq, qRT-PCR, and IHC to investigate the relationship between MTUS1/ATIP1 and FTO. MeRIP-qPCR, m^{6}A dot blot, RNA and protein stability assays, and RNC-qRT-PCR were employed to elucidate the mechanism by which FTO mediates demethylation of MTUS1/ATIP1 in HNSCC. Functional assays, subcutaneous tumorigenesis, and in situ tongue cancer models were conducted to assess the impact of the FTO-MTUS1/ATIP1 pathway on proliferative capacity of HNSCC tumors.

Results FTO was observed to be markedly upregulated and showed a negative correlation with MTUS1/ATIP1 expression in HNSCC. FTO was responsible for mediating m^{6}A demethylation in the 3'UTR of MTUS1/ATIP1, leading to its degradation. Additionally, silencing MTUS1/ATIP1 successfully reversed the tumor-promoting effects on HNSCC triggered by FTO in in vitro and in vivo.

Conclusions Our research elucidated the functional importance of FTO-mediated m^{6}A demethylation of MTUS1/ATIP1, suggesting that targeting the FTO-MTUS1/ATIP1 axis could be a prospective novel approach for treating HNSCC.

Keywords MTUS1/ATIP1, Head and neck squamous cell carcinoma, FTO, N6-methyladenosine, Demethylation

†Dongxiao Tang and Congyuan Cao contributed equally to this work.

*Correspondence:
Anxun Wang
wanganx@mail.sysu.edu.cn
[1]Department of Oral and Maxillofacial Surgery, The First Affiliated Hospital, Sun Yat-Sen University, Guangzhou, Guangdong 510080, China
[2]Department of Stomatology, The Third Affiliated Hospital, Sun Yat-Sen University, Guangzhou, Guangdong 510630, China
[3]Animal Experiment Center, The First Affiliated Hospital, Sun Yat-Sen University, Guangzhou, Guangdong 510080, China

© The Author(s) 2024. **Open Access** This article is licensed under a Creative Commons Attribution-NonCommercial-NoDerivatives 4.0 International License, which permits any non-commercial use, sharing, distribution and reproduction in any medium or format, as long as you give appropriate credit to the original author(s) and the source, provide a link to the Creative Commons licence, and indicate if you modified the licensed material. You do not have permission under this licence to share adapted material derived from this article or parts of it. The images or other third party material in this article are included in the article's Creative Commons licence, unless indicated otherwise in a credit line to the material. If material is not included in the article's Creative Commons licence and your intended use is not permitted by statutory regulation or exceeds the permitted use, you will need to obtain permission directly from the copyright holder. To view a copy of this licence, visit http://creativecommons.org/licenses/by-nc-nd/4.0/.

Background

Head and neck squamous cell carcinoma (HNSCC) has been recognized as the seventh most prevalent malignant tumor globally. It is a malignant neoplasm that arises from the mucosal epithelium of head and neck region [1, 2]. Despite advancements in current strategies for treating advanced HNSCC, the five-year overall survival rate (OS) has not seen a significant increase and remains around 50% [3]. The microtubule-associated tumor suppressor gene, known as MTUS1, is situated on chromosome 8p22. A group of proteins known as angiotensin II receptor-interacting proteins (ATIPs) is encoded by the MTUS1 gene [4–6]. Previous research conducted by our team has shown that the major isoform found in HNSCC tissues is MTUS1 transcript variant 5 (ATIP1) [5]. The decreased expression of MTUS1/ATIP1 is closely linked to the lower overall survival rates in patients with HNSCC [7]. Restoring MTUS1/ATIP1 expression has been shown to trigger cell death and reduce both proliferation and migration abilities of HNSCC cells [8]. These results suggest that MTUS1/ATIP1 may possess a potential tumor suppressor function in clinical management of HNSCC [9]. However, the reasons behind the downregulation of MTUS1/ATIP1 and its underlying mechanisms in HNSCC have not been fully elucidated.

N6-methyladenosine (m^6A) methylation, which consists of 0.1–0.4% adenylate residues, the most prevalent modification observed in mammalian messenger RNA [10]. The m^6A RNA modification is primarily regulated by three main categories of enzymes: methyltransferases, binding proteins, and demethylases [11], and it impacts RNA splicing, export, stability, translation, and degradation [12]. Research has shown that m^6A methylation is significantly involved in the progression, dissemination, and metastasis of various malignancies [13, 14]. The fat mass and obesity-related gene (FTO) functions as an m^6A demethylase and has been shown to selectively convert m^6A back to adenosine specifically within nuclear RNA. This discovery indicates the reversible nature of RNA m^6A modification [15]. Various researches had revealed abnormal expression of FTO in different malignant tumors [16, 17], strongly correlating with tumor characteristics such as oncogenesis, proliferation, and invasions [18–20].

Shi et al. revealed FTO reduces m^6A content and enhances cell proliferation of non-small cell lung cancer through activating KRAS signaling [21]. Yue et al. similarly reported The upregulation of FTO has been shown to enhance both cell proliferation and migration in the context of colorectal cancer. This phenomenon arises from the interaction between FTO and the c-myc proto-oncogene [22]. Despite these findings, research on the specific targets of FTO and its precise functions in HNSCC remains limited. Further exploration is needed to understand the epigenetic regulation of FTO in the initiation and progression of HNSCC.

To explore FTO's role in regulating mRNA of MTUS1/ATIP1 within HNSCC, we initially utilized m^6A-RNA immunoprecipitation and sequencing (MeRIP-seq) to scrutinize HNSCC tissues, revealing a significant decrease in MTUS1/ATIP1 m^6A methylation levels compared to normal tissues. Subsequent validation through qRT-PCR and immunohistochemistry staining (IHC) demonstrated elevated FTO expression levels in HNSCC, which were correlated with unfavorable overall survival outcomes among patients with HNSCC. FTO expression showed an inverse correlation with MTUS1/ATIP1 expression. Further experiments, such as MeRIP-qPCR, dual-luciferase assay, RNA and protein stability assays, and ribosome-nascent chain complex (RNC)-qRT-PCR, demonstrated that FTO modulated MTUS1/ATIP1 expression by reducing mRNA stability and translation. Overall, our research indicates that the decrease in MTUS1/ATIP1 is associated with FTO-driven m^6A demethylation in HNSCC, highlighting the potential for targeting the FTO-MTUS1/ATIP1 axis as a therapeutic strategy for HNSCC.

Methods

Tissue samples from HNSCC patients

All tissue specimens cited in this research were gathered from The First Affiliated Hospital of Sun Yat-sen University between 2016 and 2019. The collection comprised 100 HNSCC specimens and 90 paracancerous tissues located 2 cm away from HNSCC tissue. Patients who had undergone chemotherapy or radiotherapy prior to surgery were not included in the research. Before commencing the sample collection procedures, informed consent was meticulously obtained from each patient. Overall survival was computed based on the time span from the initial diagnosis until most recent follow-up in November 2023 or the time of decease. This research received authorization from the ethics board of the medical facility ([2016]074 and [2022]229).

Cell culture and transfection

HNSCC cell line HSC3 was sourced from the Japanese Collection of Research Bioresource cell bank, and HNSCC cell lines SCC9 and SCC25 were obtained from ATCC. Each cell line underwent authentication via short tandem repeat (STR) profiling.

FTO or ATIP1 short hairpin RNA (shRNA) and FTO cDNA (ID: NM_001080432) lentiviral vectors, and their respective negative control (NC) sequences were obtained from Jikai Biotechnology Co., Ltd. (Shanghai, China). MTUS1/ATIP1 cDNA (ID: NM_020749.4) and corresponding NC lentiviral vectors were obtained from iGene Co., Ltd. (Guangzhou, China). To determine the

most effective shRNA sequences for knocking down the expression of human ATIP1 or FTO, three different shRNA sequences were evaluated. Following a thorough assessment, the most potent knockdown sequence for each gene was selected for subsequent studies. Lentiviruses were used to transduce cells at an MOI of 25. The Supplementary Table S1 contains the specific shRNA sequences for FTO or MTUS1/ATIP1.

Quantitative real-time PCR (qRT–PCR)

TRIzol (ThermoFisher, 15596-018) was utilized for the isolation of RNA from tissues and cells associated with HNSCC. Following this, Takara RT kit (Takara, RR047A) was used for the reverse transcription of mRNA. This method enables the synthesis of complementary DNA from mRNA templates. The SYBR-green PCR kit (TOYOBO, QRT-201) was employed for RT-PCR analysis. The relative expression levels of all mRNAs (primers are detailed in Supplementary Table S2) were determined utilizing the $^{\Delta\Delta}$Ct method.

Western blotting

Ice-cold RIPA buffer (CST, 9806 S) was used to harvested total cellular protein from living cells. Cellular proteins were loaded onto pre-configured SDS-PAGE gels of varying concentrations for separation, followed by transfer onto PVDF membranes. Following a blocking step at RT using 3% BSA (Aladdin, B265994), the membranes were kept overnight with 1st antibodies, and subsequently exposed to 2nd antibodies. Subsequently, the membranes were rinsed 3×5 min in TBST and identified through enhanced chemiluminescence (ECL; ThermoFisher, 34580), followed by visualization using the ProteinSimple imaging system (Bio-Techne, Minneapolis, MN). The primary antibodies used in this research include ATIP1 (N-terminal region) from Aviva Systems Biology (ARP44418_T100), MTUS1 from Cell signaling Technology (CST, 13436-1-AP), FTO from Proteintech (27226-1-AP), β-Actin from CST (4970), and GAPDH from CST (2118).

RNA m^{6}A dot blot assay

RNA samples were initially subjected to a denaturation step at 95 °C for 3 min in RNA incubation buffer. The denatured samples were subsequently divided into two experimental groups, consisting of 400 ng and 200 ng, respectively, and then transferred onto Hybond-N+membranes (Beyotime, Shanghai, China). The membrane was UV cross-linked using a UV crosslinker (Spectrolinker XL-1500, Westbury, NY) at 254 nm. Following the blocking steps, the membranes were incubated with the m^{6}A antibody (Abcam, ab284130) and subsequently treated with 2nd antibodies (CST, 7074 S) for a duration of 2 h. After rinsing the membranes in TBST, dot blot intensities were detected using ECL (ThermoFisher, 34580) and visualized with the ProteinSimple imaging system (Bio-Techne, Minneapolis, MN). Subsequent staining of the membrane was was carried using a pre-diluted methylene blue working solution (MCE, HY-B1359) to determine the RNA content.

MeRIP-seq and MeRIP-qPCR

The experiments were conducted following previously published protocols with some adjustments [23–25]. Total RNA samples from HNSCC tissues in our experiment were isolated and then subjected to fragmentation using $ZnCl_2$. The RNA was subsequently treated treated with either m^{6}A antibody (Abcam, ab284130) or 2nd antibody for a duration of 2 h. Following the addition of magnetic beads (MCE, HY-K0202), we put the mixture in four-degree refrigerator for another 2 h in order to facilitate the capture of immunoprecipitated fragments. Following the purification of the fragments, they were divided into two distinct experimental groups: one portion was designated for sequencing library construction, while the other was allocated for qRT-PCR analysis. Sequencing of the RNA samples was carried out utilizing a NextSeq 500 sequencer (Illumina, Hayward, CA). The obtained data was subjected to analysis as detailed in earlier protocols. The identification of methylated sites on the RNAs (peaks) was done through the utilization of MACS software.

Immunohistochemistry (IHC) staining

Tissue sections from collected specimens were deparaffinized and rehydrated to restore their original moisture levels, followed by endogenous peroxidase quenching and antigen extraction. After the blocking step, the slides were incubated with ATIP1 (N-terminal region) (Aviva Systems Biology, ARP44418_T100) antibody or FTO (Proteintech, 27226-1-AP) antibody, and subsequently treated with a 2nd antibody. After being rinsed in PBS, sections were dyed using a DAB kit (Proteintech, PR30010) and hematoxylin. Each sample was evaluated using the scoring system describedby Pirker et al. [26]. The Immunohistochemistry score is a continuous scale (0-300), determined by multiplying the staining intensity score (0–3) with the proportion of cells corresponding to each level.

Protein and RNA stability assays

These experiments were carried out on HNSCC cells to examine how FTO influences the stability of MTUS1/ATIP1 mRNA and its corresponding protein. In the protein decay experiment, the indicated cells were exposed to cycloheximide (CHX; APExBIO, A8244-1000) at concentrations of 100 mg/mL for 0, 2, 4, and 8 h. Total cellular protein was collected, and the relative abundance of

MTUS1/ATIP1 protein (compared to 0 h) was measured through western blotting. In the RNA decay experiment, the indicated cells were exposed to ActD at concentrations of 5 mg/mL for 0, 3, and 6 h. Subsequently, the relative level of MTUS1/ATIP1 mRNA was measured via qRT-PCR.

Cell proliferation assay

The impact of FTO and MTUS1/ATIP1 on the proliferation of HNSCC cells was investigated using Cell Counting Kit-8 (CCK-8; Dojindo, Kumamoto, Japan) assays. The HNSCC cell solution was initially diluted and then seeded into a 96-well plate (3000 cells/well). The cells were allowed to incubate for 24, 48, 72, or 96 h. After a 2-hour incubation period with the CCK-8 solution, the absorbance was measured at 450 nm using a microplate reader (Bio-Tek, Winooski, VT).

Plate colony formation assay

Cells were seeded in 6-well plates at a concentration of 180 cells/mL and cultured until visible colonies formed (approximately 2 weeks). The colonies were fixed using 4% paraformaldehyde and subsequently stained with crystal violet, followed by examination and photography.

Wound healing assay

The HNSCC cell solution was initially diluted and then seeded in a 6-well plate until they reached 100% confluence. Subsequently, a fixed-width band was created by scratching using a sterile 200μL tip, followed by incubation in medium containing 2% FBS for 24 h. Wound closure of all cells in the 6-well plate was examined using the Zeiss Z1 microscope to track the migrating front.

Ribosome-nascent chain complex (RNC)-qRT-PCR assay

The ribosome-Nascent Chain Complex was extracted following established protocols with minor modifications [27]. Cycloheximide (100 mg/mL) was initially administered to HNSCC cells, followed by the addition of a ribosome buffer containing 1% Triton X-100. After a 30-minute ice bath, the lysates were centrifuged to eliminate cell debris and nuclei for a duration of ten minutes at 16,200×g and a temperature of 4 degrees Celsius.

The supernatants were subsequently gathered and placed atop 20 mL of a buffer containing 30% sucrose.

We then utilized ultracentrifugation to gather RNC under conditions of 185,000×g and 4 degrees Celsius for a duration of five hours. Finally, RNA from the polysome fraction was analyzed using qRT-PCR as described in the aforementioned methods.

Animals study

BALB/c nude mice were obtained and housed in a controlled specific pathogen-free (SPF) environment at the Animal Experiment Center affiliated with the First Affiliated Hospital of Sun Yat-sen University (Guangzhou, China). The animal experiments conducted during this research received ethical approval from the Ethics Committee of the First Affiliated Hospital of Sun Yat-sen University ([2022]229).

All models were created based on previously published methods, incorporating specific modifications [23, 28, 29]. In the subcutaneous tumorigenesis model, the indicated HNSCC SCC9 cells were injected into the right armpits of six-week-old female mice at a concentration of 1×10^6 cells in 100μL of vehicle composed of DMEM/Matrigel matrix (1:1). The sizes of the xenografts were measured, computed and recorded every three days: tumor volume (mm^3) = ½×length×$width^2$. All mice in the subcutaneous injection experimental group were euthanized were euthanized 28 days post-injection. In the in situ tongue cancer model, the indicated HNSCC SCC9 cells were injected into the right lateral tongue of six-week-old female mice at a concentration of 1×10^5 cells in 20 μL of vehicle. The xenografts were measured, computed and recorded every three days. At the 21-day observation, we found the mice weight in tongue cancer groups significantly decreased with tumor growth. Consequently, we terminated the experiment for the tongue cancer groups at that time. Following euthanasia, the tumors were dissected, weighed, measured, and subsequently embedded, sectioned, and stained. For the euthanasia procedure, the mice were placed in the euthanasia box, and carbon dioxide was gradually introduced over a period of 15 min. After euthanization by carbon dioxide asphyxiation, each mouse was individually checked, followed by cervical dislocation. The euthanasia methods employed for all mice were approved by The Ethics Committee of the First Affiliated Hospital of Sun Yat-Sen University and are in accordance with the AVMA Euthanasia Guidelines of Animals (2013 edition).

Statistical analysis

Statistical analysis of the data in all experiments was carried out utilizing GraphPad Prism v10.1 along with SPSS v27.0. The relationships between FTO and ATIP1 were evaluated through IHC scores and analyzed using Pearson's correlation coefficient. For survival analysis, a Kaplan-Meier curve was generated and accompanied by a log-rank test. Unpaired two-tailed Student's t-tests were used to assess differences between two groups. In order to evaluate variations involving multiple groups, one-way ANOVA was used. The results are presented as mean ± SD or SEM. $P<0.05$ was deemed statistically significant.

Results

Downregulation of MTUS1/ATIP1 was related to mA demethylation in HNSCC

Our previous study confirmed a notable decrease in MTUS1/ATIP1 expression in HNSCC [5, 9]. To investigate the underlying mechanism behind this downregulation, we conducted m^{6}A meRIP-seq analysis. The peaks of N6-methyladenosine were predominantly located near translation stop sites and were mainly enriched in intronic regions, with some presence in distal intergenic and promoter regions in the metagene analysis. Only a small fraction of m^{6}A peaks were observed in downstream, 5'UTR, 3'UTR, or exonic regions (Fig. 1A). No notable differences were found in m^{6}A modification when comparing the mRNA transcripts of normal tissues to those of HNSCC (Fig. 1B). Sequence analysis of the meRIP-seq data identified the consensus motif GGACU in HNSCC tissue (Fig. 1C). Visualization analysis showed that m^{6}A modifications of MTUS1/ATIP1 mRNA were predominantly enriched in normal tissues, but significantly reduced in HNSCC tissues, particularly in the 3'UTR region. MTUS1/ATIP1 3'UTR m^{6}A methylation site was pinpointed to chr8:17,502,386 – 17,502,390 using IGV visualization software (Fig. 1D).

To further investigate the demethylation of MTUS1/ATIP1 in HNSCC, the expression levels of key m^{6}A modifying enzymes were investigated and compared. The findings revealed a notable rise in the expression of METTL3, WTAP, and FTO, whereas MTUS1/ATIP1 exhibited significantly lower expression in HNSCC compared to normal tissues (Fig. 1E). Among these three proteins, METTL3 and WTAP function as methylases, suggesting that they are not responsible for the observed decrease in MTUS1/ATIP1 m^{6}A methylation levels. These findings imply that the downregulation of MTUS1/ATIP1 may be associated with FTO-mediated m^{6}A demethylation in HNSCC.

FTO exhibited a negative correlation with MTUS1/ATIP1 in HNSCC

Initially, we investigated the possible connection between FTO, the main m^{6}A demethylase, and MTUS1/ATIP1 through qRT-PCR and western blotting analysis. Our findings revealed a marked rise in both mRNA and protein levels of FTO, while MTUS1/ATIP1 levels were notably decreased in HNSCC cells compared to human oral keratinocytes (HOKs) (Fig. 2A and Figure S1).

To further corroborate these findings, immunohistochemistry (IHC) staining for FTO and MTUS1/ATIP1 was performed on 100 HNSCC and 90 adjacent noncancerous tissues collected from the First Affiliated Hospital of Sun Yat-sen University. The analysis revealed a predominant nuclear expression of FTO, which showed a significant increase in HNSCC tissues (Fig. 2B-C). Area under the ROC curve (AUC) of FTO was 0.761. A threshold value of 115.5 was utilized to distinguish between patients with high and low FTO expression in cases of HNSCC (Supplementary Table S3). Elevated levels of FTO expression showed a positive correlation with the clinical phenotype of HNSCC, including advanced tumor stage (T_{3+4} versus T_{1+2}), pathological grade (Well versus Moderate/Poor), and lymph node metastasis (LN+versus LN-) (Fig. 2D-E; Supplementary Table S4). Kaplan-Meier analysis indicated that patients exhibiting higher levels of FTO expression experienced significantly shorter overall survival times in comparison to those with lower levels of FTO expression (Fig. 2F). Both univariate and multivariate analyses validated the expression level of FTO as a prognostic indicator for 5-year overall survival in HNSCC patients (Supplementary Table S5). Additionally, a notable inverse relationship was found between the FTO IHC level and the MTUS1/ATIP1 IHC level in HNSCC tissue samples (Fig. 2G).

MTUS1/ATIP1 downregulation was mediated through FTO-m^{6}A-dependent mechanism in HNSCC

To evaluate whether the expression of MTUS1/ATIP1 is influenced by the m^{6}A eraser FTO in HNSCC, we assessed the expression levels of MTUS1/ATIP1 in FTO-overexpressed or FTO-knockdowned HNSCC cells (Figure S2). The results presented in Fig. 3A-B indicated the overexpression of FTO notably reduced MTUS1/ATIP1 expression, whereas knockdown of FTO resulted in an increase in MTUS1/ATIP1 expression in HNSCC cells. Subsequent dot blot assays demonstrated that m^{6}A methylation levels decreased upon FTO overexpression (Fig. 3C) and increased after FTO silencing (Fig. 3D). Furthermore, MeRIP-qRT-PCR analysis indicated a significant reduction in MTUS1/ATIP1 m^{6}A modification following FTO overexpression (Fig. 3E), and an increase upon FTO knockdown (Fig. 3F).

To further evaluate the necessity of m^{6}A modifications on mRNAs, dual-luciferase assays were carried out. Compared to the control, overexpression of FTO significantly decreased the luciferase activity of the wild-type 3' UTR reporter construct of MTUS1/ATIP1. This effect was reversed when the sites were mutated (Fig. 3G). These findings suggest the expression of MTUS1/ATIP1 may be regulated via an FTO-m^{6}A-dependent mechanism.

FTO decreased MTUS1/ATIP1 mRNA stability and translation

To investigate the impact of m^{6}A demethylation on MTUS1/ATIP1 mRNA and protein stability, actinomycin D and cycloheximide assays were utilized. The results in Fig. 4A indicated a notable decrease in the stability of MTUS1/ATIP1 mRNA levels in FTO-overexpressed cells compared to control cells, while the degradation rate

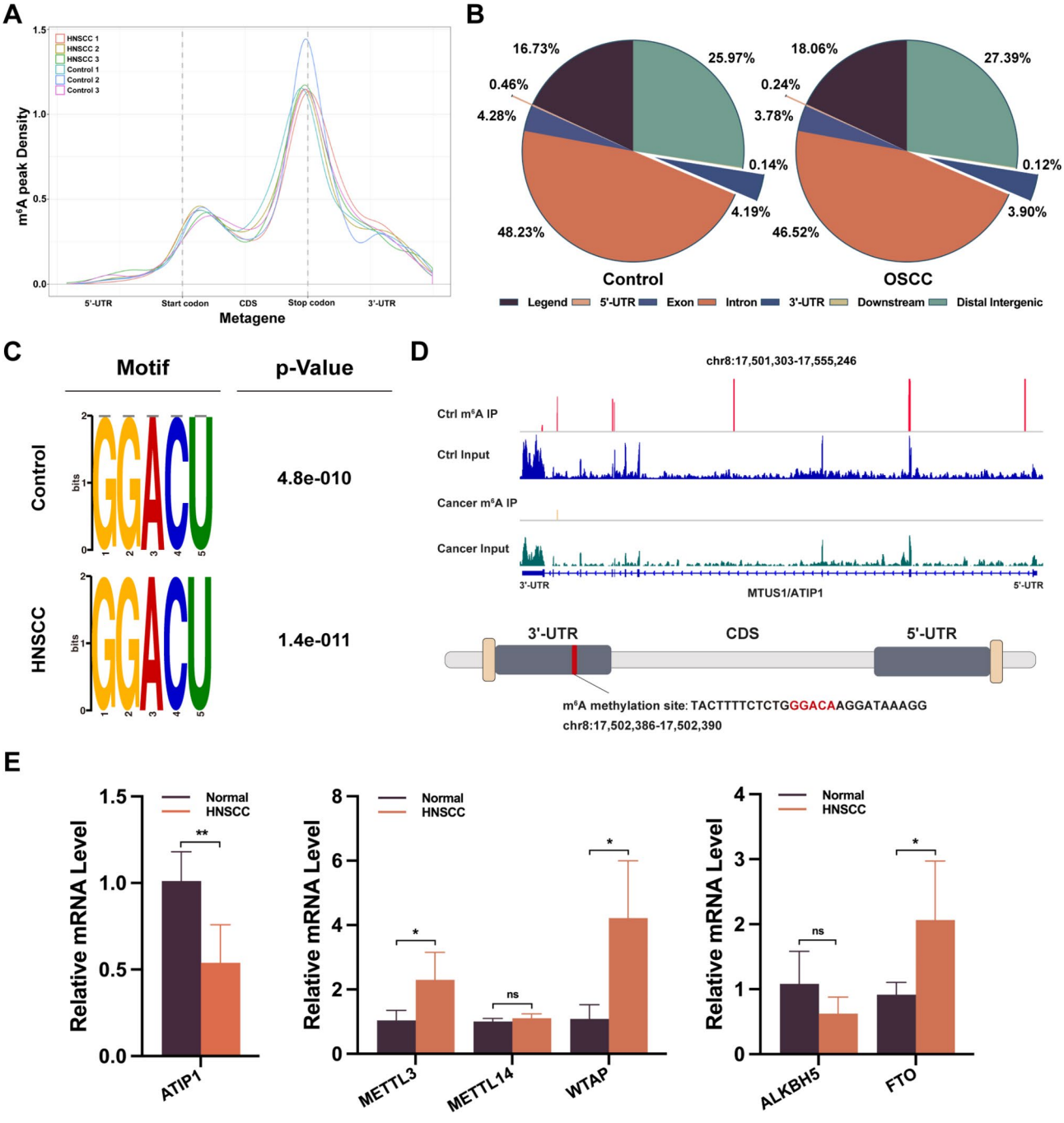

Fig. 1 Downregulation of MTUS1/ATIP1 was related to m^{6}A methylation enzymes in HNSCC. **A** The density distribution of m^{6}A peaks across mRNA transcripts was analyzed by dividing the upstream untranslated region (5'UTR), coding region (CDS), and downstream untranslated region (3'UTR) into 100 segments. The percentages of peaks within each segment were then calculated. **B** The distribution of m^{6}A peaks across the various regions of mRNA transcripts, including the 5'UTR), start codon, CDS, stop codon, and 3'UTR, is presented for the entire set of mRNA transcripts. **C** The m^{6}A motif was detected using the HOMER motif discovery tool in conjunction with meRIP-seq data. The metagene plot illustrates that the distributions of m^{6}A peaks remain largely unchanged, revealing similar GGACU consensus motifs in both HNSCC tissues and normal tissues. **D** The visualization of m^{6}A peaks from MeRIP-seq in HNSCC tissues compared to normal tissues is presented using Integrative Genomics Viewer (IGV) plots. The m^{6}A peaks are located within the 3' untranslated region (3'UTR) of the MTUS1/ATIP1 gene. A schematic representation of the m^{6}A methylation site within the 3'UTR region of MTUS1/ATIP1 is provided. **E** qRT-PCR of HNSCC tissues and adjacent normal tissues confirmed that MTUS1/ATIP1 was significantly downregulated and m^{6}A writers METTL3, and WTAP were regulated in HNSCC; erasers, FTO was significantly upregulated, while ALKBH5 expression was unchanged in HNSCC. GAPDH was used as loading proteins. *$P < 0.05$; **$P < 0.01$; ***$P < 0.001$

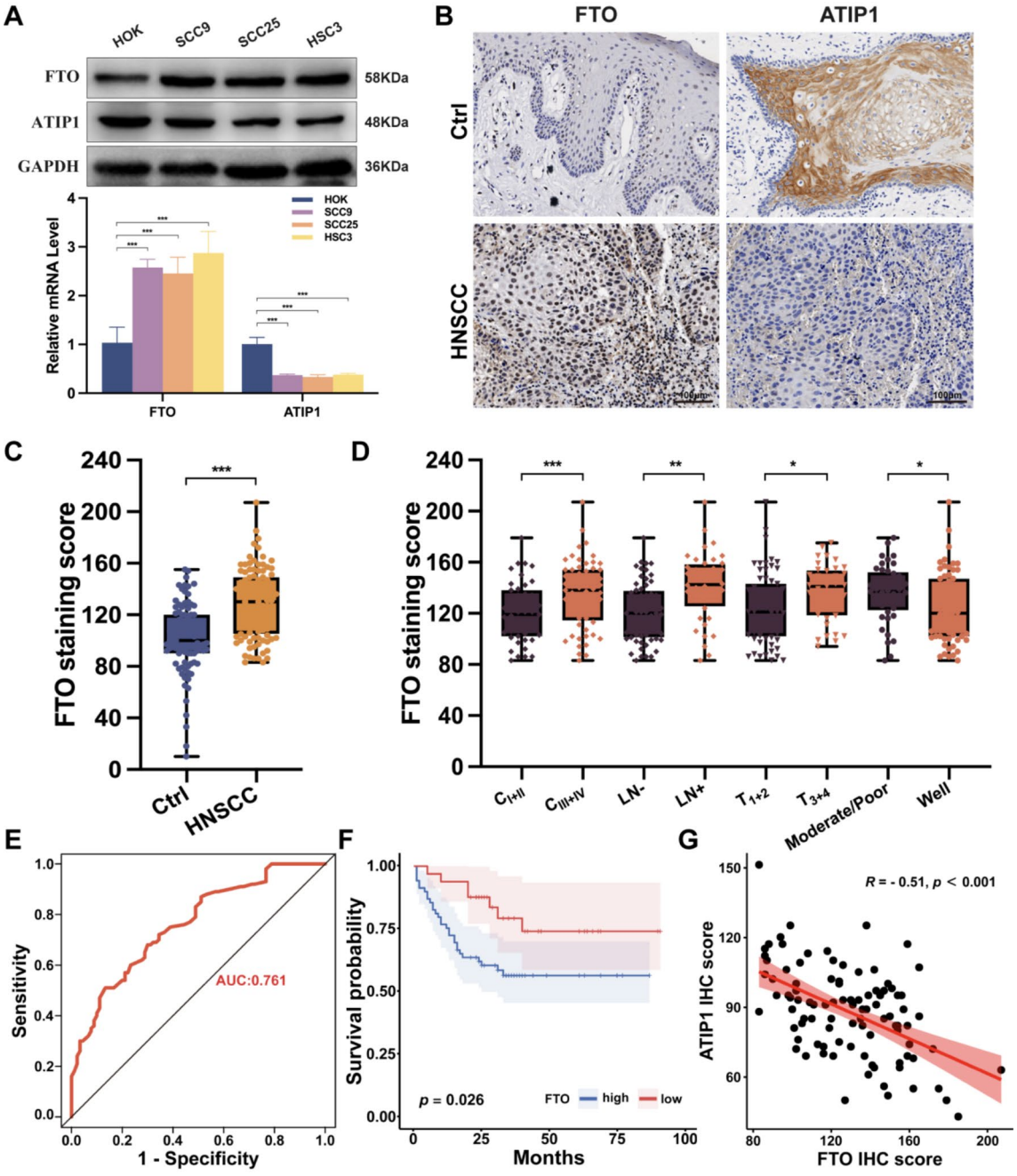

Fig. 2 FTO exhibited a negative correlation with MTUS1/ATIP1 in HNSCC. **A** The expression level of FTO and MTUS1/ATIP1 in human normal oral keratinocytes (HOKs) and HNSCC cells. **B** IHC staining for FTO or MTUS1/ATIP1 in HNSCC and normal oral mucous samples. **C** FTO IHC scores in normal oral mucosa tissue (ctrl) and HNSCC tissues. **D** FTO IHC scores in HNSCC tissues stratified by stratified by clinical stage (C_{III+IV} versus C_{I+II}), tumor stage (T_{3+4} versus T_{1+2}), lymph node metastasis (LN + versus LN-), and Pathological grade (Moderate/Poor versus Well). **E** ROC curves analyzing the potential value of FTO expression level in HNSCC diagnosis. **F** Kaplan-Meier survival curves of overall survival (OS) based on FTO expression level. **G** The correlation between the FTO protein level and the MTUS1/ATIP1 protein level in HNSCC tissue was analyzed by a Spearman's test. GAPDH was used as loading proteins. Scale bar, 100 μm. *$P < 0.05$; **$P < 0.01$; ***$P < 0.001$

of MTUS1/ATIP1 protein levels remained unchanged (Fig. 4B). Knockdown of FTO did not affect the protein degradation rate either (Fig. 4C). Furthermore, a Ribosome-Nascent Chain Complex (RNC)-qRT-PCR analysis was employed to evaluate the translation capability of MTUS1/ATIP1 mRNA. The data revealed that FTO overexpression led to a reduction in the proportion of MTUS1/ATIP1 mRNA in actively translated polysome fractions, whereas FTO knockdown had the opposite effect (Fig. 4D). These findings indicate FTO affects

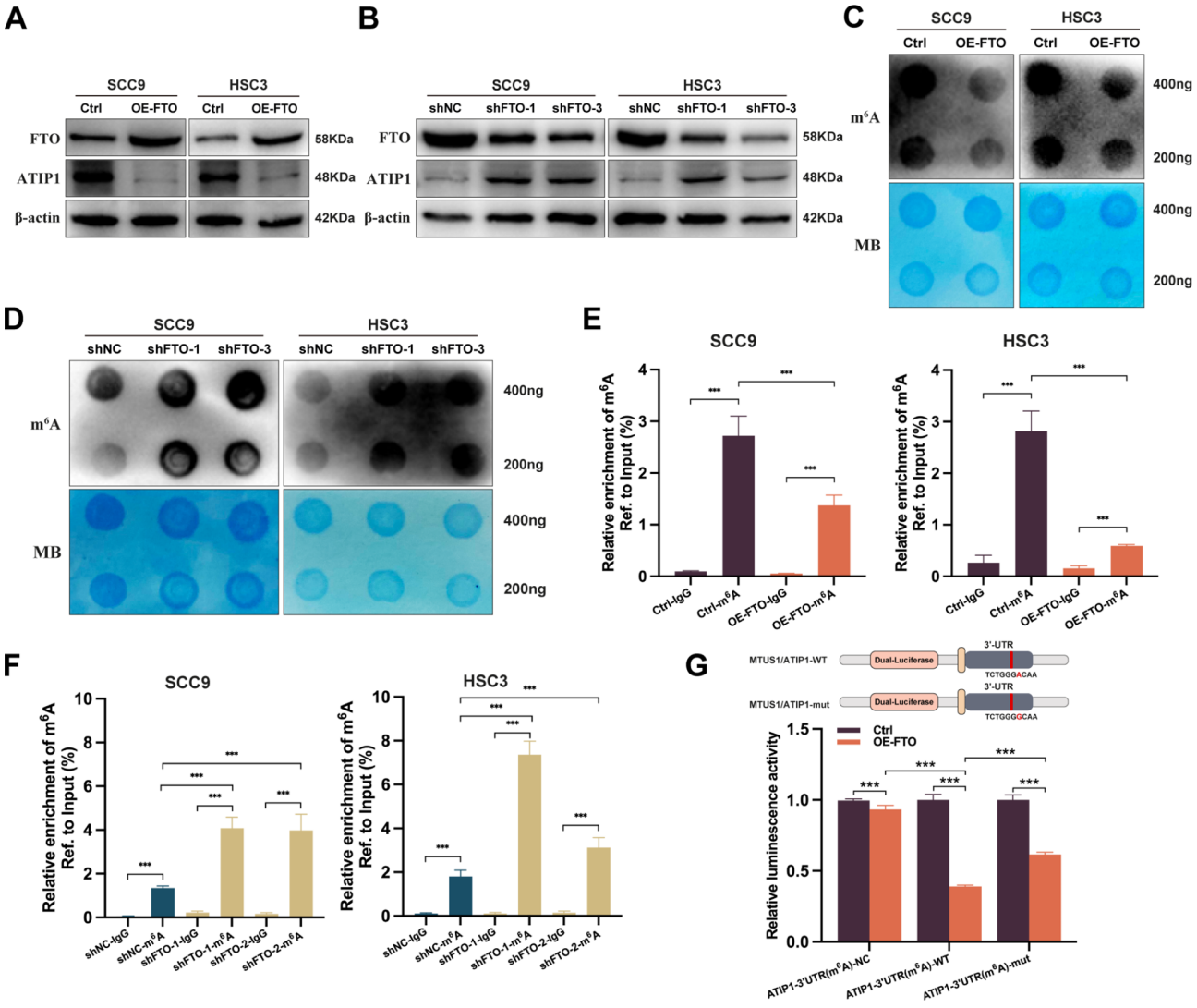

Fig. 3 MTUS1/ATIP1 downregulation was mediated through FTO-m^{6}A-dependent mechanism. **A-B** FTO and ATIP1 protein level were detected by western blotting in FTO-overexpressed (**A**) or -knockdowned (**B**) HNSCC cells. **C-D** The m^{6}A level of RNA were detected by dot blot in FTO-overexpressed (**C**) or -knockdowned (**D**) HNSCC cells. **E** MeRIP-qPCR showed that relative MTUS1/ATIP1 m^{6}A level was significantly decreased after FTO overexpression in HNSCC cells. **F** MeRIP-qPCR showed that relative MTUS1/ATIP1 m^{6}A level was significantly increased after FTO knockdown in HNCSS cells. **G** Dual-luciferase assays showed that FTO overexpression inhibited the luciferase activity of individual reporter constructs containing wild-type 3'UTR fragment of MTUS1/ATIP1, while was abrogated when the m^{6}A sites were mutated. β-actin was used as loading proteins. All data are presented as the mean ± SEM of three independent experiments. ***$P < 0.001$

MTUS1/ATIP1 expression by influencing mRNA stability and translation in HNSCC.

MTUS1/ATIP1 significantly alleviated the inhibitory effects of FTO in HNSCC in vitro and in vivo

Initially, we assessed the effect of FTO in HNSCC. As shown in Fig. 5A-F and Figure S3-S4, knockdown of FTO resulted in a reduction in the proliferative capacity, migration ability, and colony formation of HNSCC cells. Co-transfection of ATIP1 shRNA successfully reversed the inhibitory effects of FTO. Additionally, the expression levels of MTUS1/ATIP1 were elevated in HNSCC cells with FTO knockdown, but this effect was alleviated upon co-transfection with ATIP1 shRNA (Fig. 5G).

To investigate the impact of the FTO-MTUS1/ATIP1 pathway on tumor proliferative capacity in vivo, a subcutaneous tumorigenesis model was utilized. Stable FTO-knockdown or FTO/ATIP1 double knockdown cells were injected into Balb/c mice. The xenografts were measured and recorded every three days. The results showed that FTO-knockdown led to a notable reduce in both the weight and volume of tumors when compared to the control group. MTUS1/ATIP1 knockdown was able to counteract the effects of shFTO in the subcutaneous tumorigenesis model (Fig. 5H and Figure S5A).

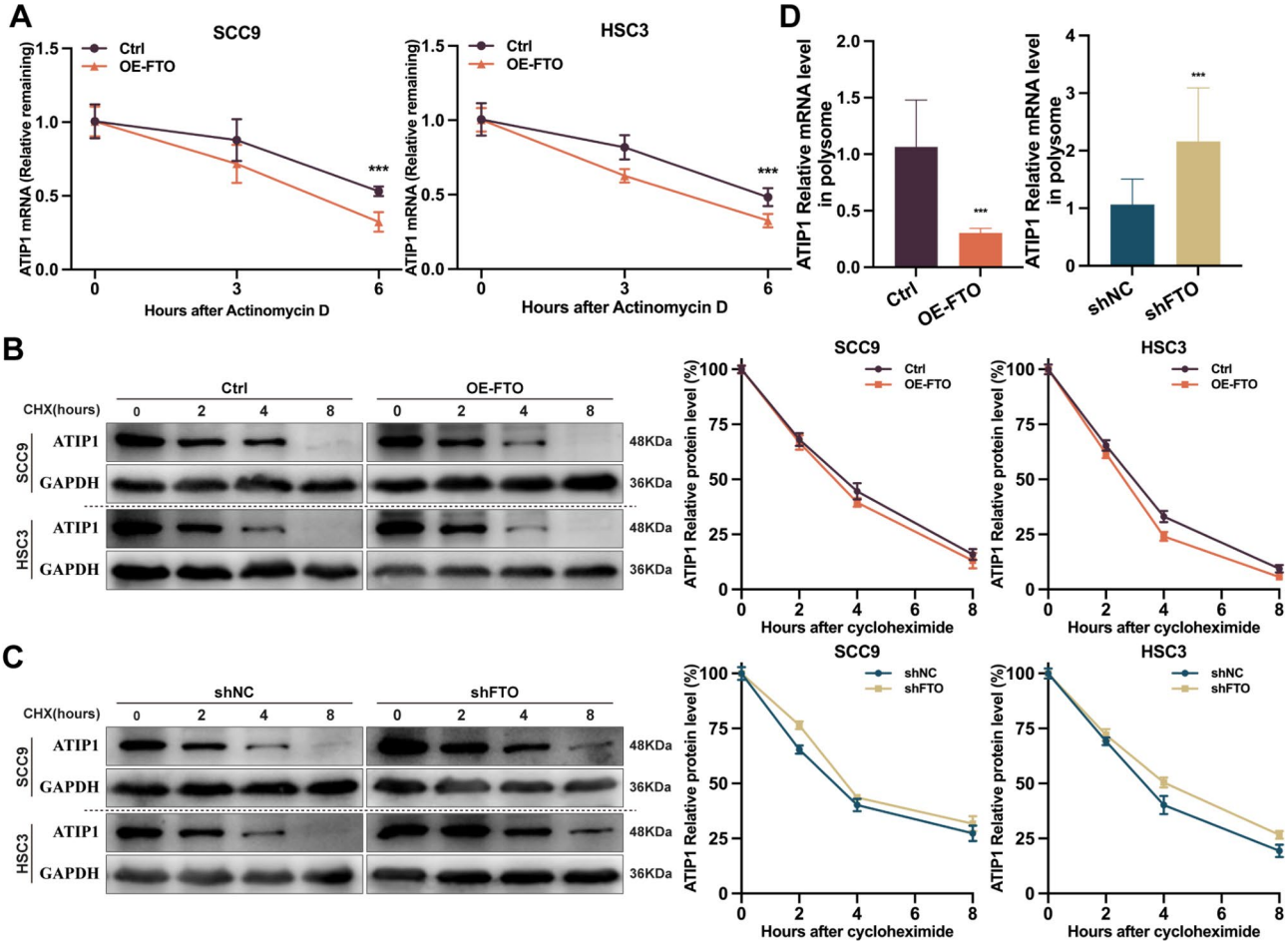

Fig. 4 FTO decreased MTUS1/ATIP1 mRNA stability and translation. **A** MTUS1/ATIP1 mRNA stability was significantly decreased in FTO-overexpressed HNSCC cells after treated with actinomycin D. **B-C** MTUS1/ATIP1 protein stability was no significant changes between FTO-overexpressed (B) or -knockdowned (C) HNSCC cells and their control cells by cycloheximide assay. **D** Polysome-fractionated samples analyzed by qRT-PCR showed that polysome-bound MTUS1/ATIP1 mRNA levels were significantly decreased after FTO overexpression in HNSCC cells, while knockdown of FTO exerted the opposite effects. GAPDH was used as loading proteins. All data are presented as the mean ± SEM of three independent experiments. ***$P < 0.001$

An in situ tongue cancer model was established using stable FTO-knockdown or double knockdown cells (shFTO and shATIP1) in HNSCC cells. The mice and the xenografts were observed every three days. Compared to the control group, the FTO-knockdown group exhibited a notable decrease in both the weight and volume of tumors. Co-transfection of ATIP1 shRNA successfully alleviated the inhibitory effects of FTO (Fig. 5I and Figure S5B). These results were in line with those observed in the subcutaneous tumor model. Collectively, these findings indicate that silencing MTUS1/ATIP1 can effectively counteract the FTO-induced inhibition of tumor growth in HNSCC, both in vitro and in vivo.

Discussion

Microtubule-associated tumor suppressor gene (MTUS1) has reduced expression in various malignancies including gastric cancer [30], colorectal carcinoma [31] and breast cancer [32]. ATIP1 is the fifth transcript variant and the predominant isoform of MTUS1, playing a vital role role in the occurrence and development of of various cancers [33]. Prior studies conducted by our team have shown a marked decrease in the expression levels of MTUS1/ATIP1 within HNSCC cells [5, 9]. MTUS1/ATIP1, acting as a tumor suppressor gene, exhibits significant antitumor activity [7, 34]. However, the reasons behind the downregulation of MTUS1/ATIP1 and its underlying mechanism in HNSCC remain unclear. This study utilized MeRIP-seq analysis of HNSCC tissues and found a significant reduction in m^6A methylation of MTUS1/ATIP1 in HNSCC, shedding light on potential m^6A-related mechanisms for the decreased expression of MTUS1/ATIP1 in this type of cancer.

N6-methyladenosine (m^6A) modification represents a crucial and widespread internal alteration found in human mRNA molecules, influencing mRNA splicing, stability, degradation, and translation [35, 36]. Research has shown that the improper regulation of m^6A

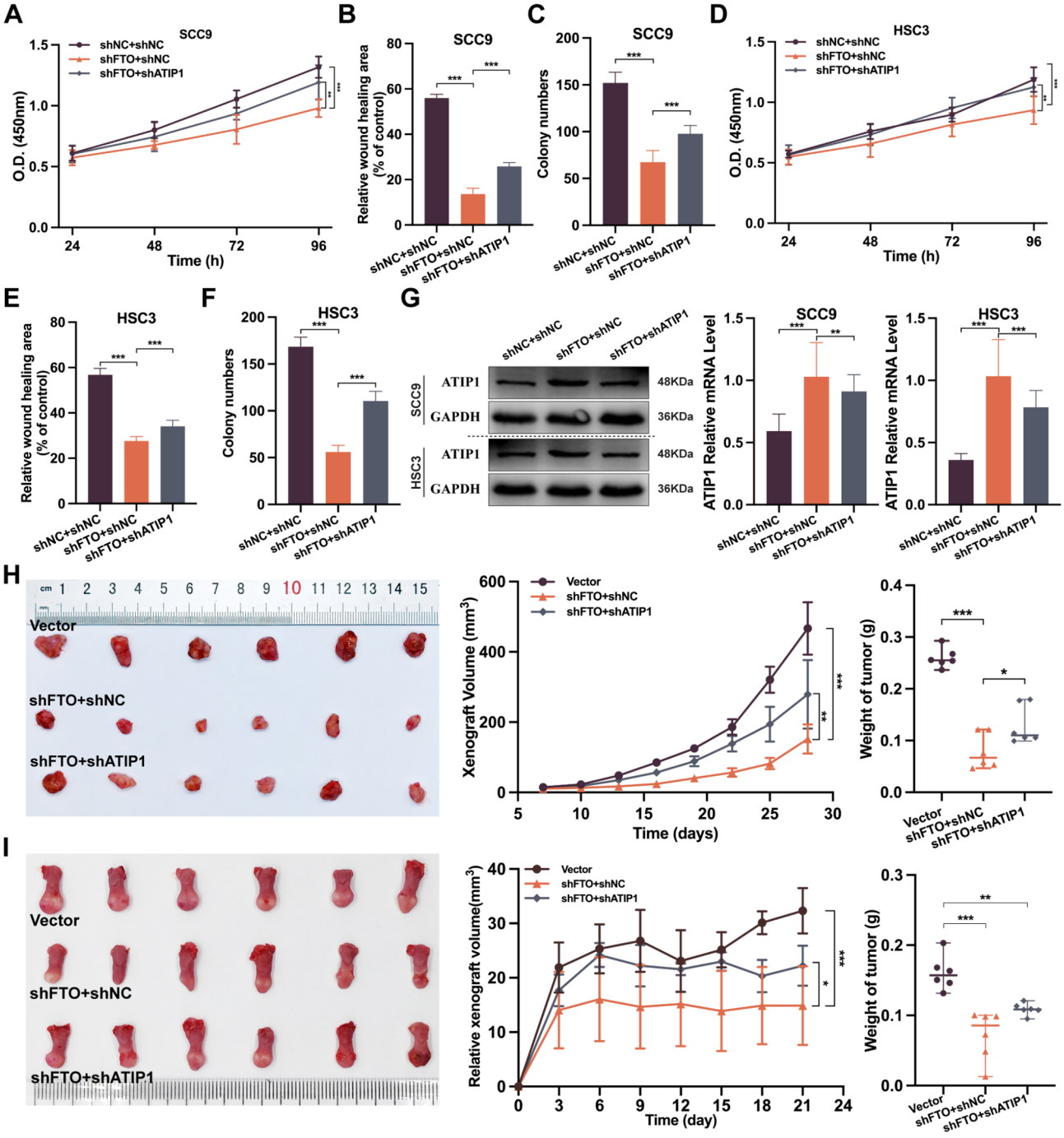

Fig. 5 MTUS1/ATIP1 significantly alleviated the inhibitory effects of FTO in HNSCC in vitro and *in vivo*. **A-C** FTO knockdown suppressed cell proliferation, migration, and colony formation in SCC9 cells. MTUS1/ATIP1 knockdown effectively reversed these effects, increasing the abilities of FTO-knockdown SCC9 cells to proliferate, migrate, and form colonies. **D-F** MTUS1/ATIP1 knockdown was found to mitigate the impact of FTO in HSC3 cells. **G** MTUS1/ATIP1 protein and mRNA level were detected after knockdown of MTUS1/ATIP1 in FTO-knockdowned HNSCC cells. **H** Knockdown of MTUS1/ATIP1 effectively promoted FTO-knockdown tumor growth of subcutaneous xenograft in mice ($n=6$). **I** Knockdown of ATIP1 effectively promoted FTO-knockdown in situ tongue tumor growth in mice ($n=6$). GAPDH was used as loading proteins. All data are presented as the mean ± SEM of three independent experiments. $^{*}P<0.05$; $^{**}P<0.01$; $^{***}P<0.001$

modification is implicated in a variety of diseases, such as brain developmental abnormalities and cancers [37]. Our previous paper has demonstrated a significant association between m^{6}A methylation and HNSCC [23, 24]. FTO, recognized as the inaugural m^{6}A demethylase, has been revealed to act as an oncogene across various cancer subtypes, with its oncogenic function relying on its demethylase activity. According to the findings of Yang

and colleagues, elevated expression of FTO in melanoma is associated with enhanced tumor growth and a reduced efficacy of anti-PD-1 blockade immunotherapy, which occurs through FTO-mediated m^{6}A demethylation [38]. Jeschke et al. observed that the suppression of FTO-mediated m^{6}A demethylase promoted the progression of epithelial tumors through epithelial-mesenchymal transition (EMT) [39]. However, there are relatively few studies focus on the FTO targets and their definitive roles in HNSCC. Wang et al. demonstrated that FTO enhances sensitivity of HNSCC to ferroptosis by suppressing ACSL3 and GPX4 [40]. Li el al. reported that FTO regulated tumorigenesis of arecoline-promoted human oral carcinoma [41]. The findings of this research reveal a strong association between elevated levels of FTO expression and poor overall survival (OS) in HNSCC patients. Furthermore, a negative relationship was identified between the expression levels of MTUS1/ATIP1 and FTO.

The carcinogenic effects of FTO are believed to stem from two main mechanisms. By modulating its demethylase activity, FTO can either enhance the translation of oncogenes or promote the degradation of tumor suppressor transcripts [42, 43]. There have been limited studies on the decay of tumor suppressor transcripts [44]. Liu et al. discovered that FTO expression is increased in Acute Myeloid Leukemia (AML), facilitating the transformation of AML cells and the process of leukemogenesis by diminishing the m^{6}A levels and destabilizing the mRNA of ASB2 and RARA [19]. Furthermore, FTO was found to accelerate the proliferation, metastasis, and colony formation abilities by influencing the mRNA stability of BNIP3 in breast cancer [45]. To clarify the molecular mechanism through which FTO influences MTUS1/ATIP1, we discovered a possible m^{6}A site located in MTUS1/ATIP1 3'UTR. We further confirmed that this site is essential for regulating the stability of MTUS1/ATIP1 mRNA through a dual-luciferase assay. Overexpression of FTO led to a reduction in both the mRNA stability and protein level of MTUS1/ATIP1 without affecting its protein degradation rate. These results align with previous findings that the mRNA stability of tumor suppressor genes in AML and breast cancer is negatively regulated by FTO [19, 45]. Additionally, the level of polysome-bound MTUS1/ATIP1 mRNA decreased in FTO-overexpressing HNSCC cells, indicating that FTO may control both the translation and stability of MTUS1/ATIP1 mRNA (Fig. 6). In order to explore the function of MTUS1/ATIP in FTO-dependent tumor growth and progression in HNSCC, shRNA targeting ATIP1 was introduced in FTO stable knockdown HNSCC cells. The experimental results demonstrated that silencing

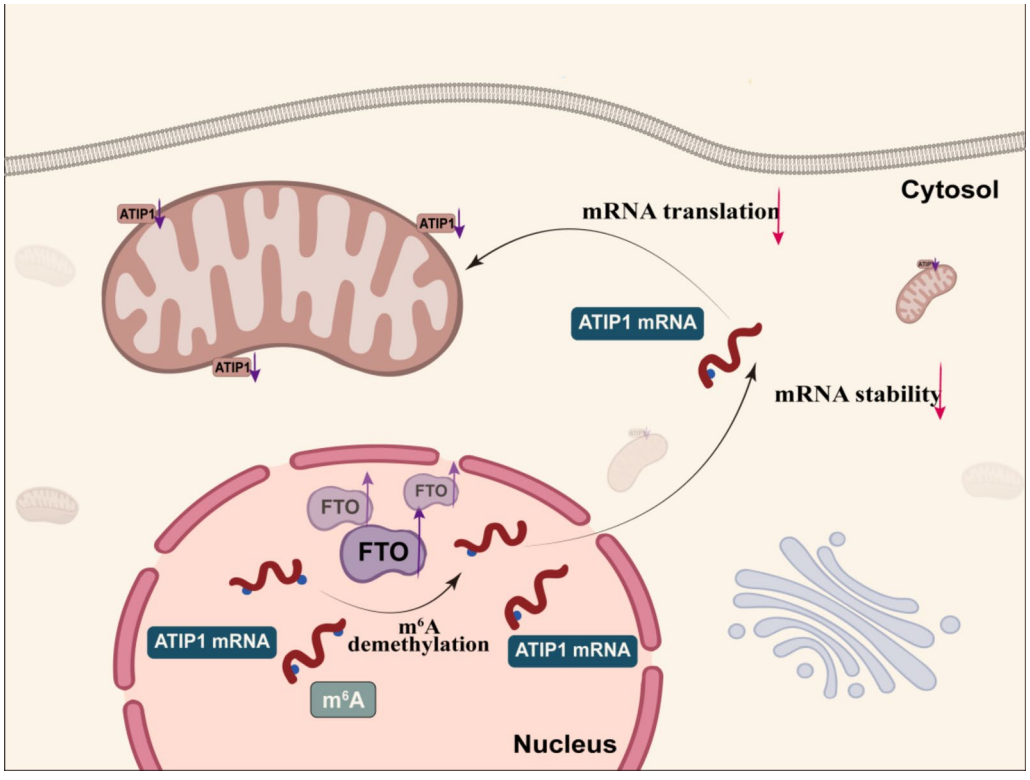

Fig. 6 Schematic diagram illustrates the mechanism by which FTO mediates the m^{6}A demethylation of MTUS1/ATIP1. FTO is significantly upregulated in HNSCC, resulting in the m^{6}A demethylation of MTUS1/ATIP1 mRNA. This demethylation leads to a marked reduction in both the stability and translational efficiency of MTUS1/ATIP1 mRNA, ultimately resulting in decreased expression of the mitochondrial outer membrane protein MTUS1/ATIP1

of MTUS1/ATIP1 effectively counteracted the effects of shFTO on tumor growth, both in vitro and in vivo, highlighting MTUS1/ATIP1 as a downstream target of FTO in regulating HNSCC growth and progression. In previous studies, we demonstrated that MTUS1/ATIP1 is localized in the outer mitochondrial membrane, influences mitochondrial function and metabolism, and induces pyroptotic death in HNSCC cells via the ROS-BAX-caspase-9/-3-GSDME pathway [9]. This study further elucidates the FTO demethylation mechanism associated with the decline of MTUS1/ATIP1, revealing a previously unrecognized gene regulatory mechanism in HNSCC and providing significant insights into the molecular mechanisms underlying tumorigenesis. Moreover, considering the critical role of FTO in the occurrence and progression of HNSCC, targeting FTO signaling through selective inhibitors to modulate the expression of MTUS1/ATIP1 may represent a promising therapeutic strategy for treating HNSCC. Given that FTO-driven demethylation is also implicated in other cancer types, our findings could have far-reaching implications for cancer biology and treatment.

Conclusions

This study reveals that elevated FTO expression correlates with poor overall survival in HNSCC and negatively regulates MTUS1/ATIP1 expression by affecting mRNA stability and translation. Silencing MTUS1/ATIP1 counteracts FTO-driven tumor growth in vitro and *in vivo*, highlighting the role of FTO-mediated m^6A demethylation in malignancy progression and identifying the FTO-MTUS1/ATIP1 pathway as a potential therapeutic target.

Abbreviations

ATIP	AT2 receptor-interacting protein
MTUS1	Microtubule-associated tumor suppressor gene
FTO	Fat mass and obesity-associated protein
HNSCC	Head and neck squamous cell carcinoma
M^6A	N6-methyladenosine
MeRIP	M^6A-RNA immunoprecipitation
qRT-PCR	quantitative real-time PCR
IHC	Immunohistochemistry staining
OS	Overall survival
RNC	Ribosome-nascent chain complex
MOI	Multiplicity of infection
FBS	Foetal bovine serum
shRNA	Short hairpin RNA
CHX	Cycloheximide
ActD	Actinomycin D
CCK-8	Cell counting kit-8
SPF	Specific pathogen free
ROC curve	Receiver operating characteristic curve
TCGA	The Cancer Genome Atlas

Supplementary Information

The online version contains supplementary material available at https://doi.org/10.1186/s12885-024-13253-y.

Supplementary Material 1

Supplementary Material 2

Acknowledgements

Not applicable.

Author contributions

AXW conceived of, designed, and supervised the study. DXT performed most of the experiments, analyzed the results and wrote the manuscript. CYC collected the tumour samples and performed some of the experiments. WGL and DXT established HNSCC CDX models. WGL provided technical assistance with the experiments. All authors read and approved this version of the manuscript.

Funding

This work was supported by funding from the National Nature Science Foundation of China (grant Nos. 82173041, 82372868).

Data availability

Raw sequencing data were accessed via the Chinese Academy of Science's Genome Sequence Archive (GSA) for Human (https://bigd.big.ac.cn/gsa-human/browse/HRA008126) with the accession number HRA008126. All the other data supporting the findings of this study are available from the corresponding author upon reasonable request.

Declarations

Ethics approval and consent to participate

The Ethics Committee of the First Affiliated Hospital of Sun Yat-Sen University approved the animal experiments ([2022]229). All samples were obtained with informed consent and the use was approved by the Institutional Review Board of the First Affiliated Hospital of Sun Yat-Sen University ([2016]074 and [2022]229).

Consent for publication

Not applicable.

Competing interests

The authors declare no competing interests.

Received: 8 July 2024 / Accepted: 26 November 2024
Published online: 03 December 2024

References

1. Chen C-H, Chang AYW, Li S-H, Tsai H-T, Shiu L-Y, Su L-J, et al. Suppression of Aurora-A-FLJ10540 signaling axis prohibits the malignant state of head and neck cancer. Mol Cancer. 2015;14:83.
2. Sung H, Ferlay J, Siegel RL, Laversanne M, Soerjomataram I, Jemal A, et al. Global Cancer statistics 2020: GLOBOCAN estimates of incidence and Mortality Worldwide for 36 cancers in 185 countries. CA Cancer J Clin. 2021;71:209–49.
3. Attademo L, Tuninetti V, Pisano C, Cecere SC, Di Napoli M, Tambaro R, et al. Immunotherapy in cervix cancer. Cancer Treat Rev. 2020;90:102088.
4. Seibold S, Rudroff C, Weber M, Galle J, Wanner C, Marx M. Identification of a new tumor suppressor gene located at chromosome 8p21.3-22. FASEB J. 2003;17:1180–2.
5. Ding X, Zhang N, Cai Y, Li S, Zheng C, Jin Y, et al. Down-regulation of tumor suppressor MTUS1/ATIP is associated with enhanced proliferation, poor differentiation and poor prognosis in oral tongue squamous cell carcinoma. Mol Oncol. 2012;6:73–80.
6. Benedetto MD, Bièche I, Deshayes F, Vacher S, Nouet S, Collura V, et al. Structural organization and expression of human MTUS1, a candidate 8p22 tumor suppressor gene encoding a family of angiotensin II AT2 receptor-interacting proteins, ATIP. Gene. 2006;380 2:127–36.
7. Zhao T, Ding X, Chang B, Zhou X, Wang A. MTUS1/ATIP3a down-regulation is associated with enhanced migration, invasion and poor prognosis in salivary adenoid cystic carcinoma. BMC Cancer. 2015;15:203.

8. Zhao T, He Q, Liu Z, Ding X, Zhou X, Wang A, Angiotensin. II type 2 receptor-interacting protein 3a suppresses proliferation, migration and invasion in tongue squamous cell carcinoma via the extracellular signal-regulated kinase-Snai2 pathway. Oncol Lett. 2016;11 1:340–4.
9. Tang D, Zhao L, Huang S, Li W, He Q, Wang A. Mitochondrial outer membrane protein MTUS1/ATIP1 exerts antitumor effects through ROS-induced mitochondrial pyroptosis in head and neck squamous cell carcinoma. Int J Biol Sci. 2024;20.
10. An Y, Duan H. The role of m6A RNA methylation in cancer metabolism. Mol Cancer. 2022;21:14.
11. He L, Li H, Wu A, Peng Y, Shu G, Yin G. Functions of N6-methyladenosine and its role in cancer. Mol Cancer. 2019;18:176.
12. Lan Q, Liu PY, Haase J, Bell JL, Hüttelmaier S, Liu T. The critical role of RNA m6A methylation in Cancer. Cancer Res. 2019;79:1285–92.
13. Li H-B, Tong J, Zhu S, Batista PJ, Duffy EE, Zhao J, et al. m6A mRNA methylation controls T cell homeostasis by targeting the IL-7/STAT5/SOCS pathways. Nature. 2017;548:338–42.
14. Weng H, Huang H, Wu H, Qin X, Zhao BS, Dong L, et al. METTL14 inhibits hematopoietic Stem/Progenitor differentiation and promotes Leukemogenesis via mRNA m6A modification. Cell Stem Cell. 2018;22:191–e2059.
15. Jia G, Fu Y, Zhao X, Dai Q, Zheng G, Yang Y, et al. N6-methyladenosine in nuclear RNA is a major substrate of the obesity-associated FTO. Nat Chem Biol. 2011;7:885–7.
16. Zhou S, Bai Z-L, Xia D, Zhao Z-J, Zhao R, Wang Y-Y, et al. FTO regulates the chemo-radiotherapy resistance of cervical squamous cell carcinoma (CSCC) by targeting β-catenin through mRNA demethylation. Mol Carcinog. 2018;57:590–7.
17. Zhang L, Wan Y, Zhang Z, Jiang Y, Lang J, Cheng W, et al. FTO demethylates m6A modifications in HOXB13 mRNA and promotes endometrial cancer metastasis by activating the WNT signalling pathway. RNA Biol. 2021;18:1265–78.
18. Shimura T, Kandimalla R, Okugawa Y, Ohi M, Toiyama Y, He C, et al. Novel evidence for m6A methylation regulators as prognostic biomarkers and FTO as a potential therapeutic target in gastric cancer. Br J Cancer. 2022;126:228–37.
19. Li Z, Weng H, Su R, Weng X, Zuo Z, Li C, et al. FTO plays an oncogenic role in Acute myeloid leukemia as a N6-Methyladenosine RNA demethylase. Cancer Cell. 2017;31:127–41.
20. Li Y, Su R, Deng X, Chen Y, Chen J. FTO in cancer: functions, molecular mechanisms, and therapeutic implications. Trends Cancer. 2022;8:598–614.
21. Shi H, Zhao J, Han L, Xu M, Wang K, Shi J, et al. Retrospective study of gene signatures and prognostic value of m6A regulatory factor in non-small cell lung cancer using TCGA database and the verification of FTO. Aging. 2020;12:17022–37.
22. Yue C, Chen J, Li Z, Li L, Chen J, Guo Y. microRNA-96 promotes occurrence and progression of colorectal cancer via regulation of the AMPKα2-FTO-m6A/MYC axis. J Exp Clin Cancer Res. 2020;39:240.
23. Liu L, Wu Y, Li Q, Liang J, He Q, Zhao L, et al. METTL3 promotes tumorigenesis and metastasis through BMI1 m6A methylation in oral squamous cell carcinoma. Mol Ther. 2020;28:2177–90.
24. Chen J, Li S, Huang Z, Cao C, Wang A, He Q. METTL3 suppresses anlotinib sensitivity by regulating m6A modification of FGFR3 in oral squamous cell carcinoma. Cancer Cell Int. 2022;22:295.
25. Dominissini D, Moshitch-Moshkovitz S, Salmon-Divon M, Amariglio N, Rechavi G. Transcriptome-wide mapping of N(6)-methyladenosine by m(6)A-seq based on immunocapturing and massively parallel sequencing. Nat Protoc. 2013;8:176–89.
26. Pirker R, Pereira JR, von Pawel J, Krzakowski M, Ramlau R, Park K, et al. EGFR expression as a predictor of survival for first-line chemotherapy plus cetuximab in patients with advanced non-small-cell lung cancer: analysis of data from the phase 3 FLEX study. Lancet Oncol. 2012;13:33–42.
27. Esposito AM, Mateyak M, He D, Lewis M, Sasikumar AN, Hutton J et al. Eukaryotic polyribosome profile analysis. J Vis Exp. 2010;:1948.
28. Chen J, Li K, Chen J, Wang X, Ling R, Cheng M, et al. Aberrant translation regulated by METTL1/WDR4-mediated tRNA N7-methylguanosine modification drives head and neck squamous cell carcinoma progression. Cancer Commun (Lond). 2022;42:223–44.
29. Tu NH, Jensen DD, Anderson BM, Chen E, Jimenez-Vargas NN, Scheff NN, et al. Legumain induces oral Cancer Pain by Biased Agonism of protease-activated Receptor-2. J Neurosci. 2021;41:193–210.
30. Li X, Liu H, Yu T, Dong Z, Tang L, Sun X. Loss of MTUS1 in gastric cancer promotes tumor growth and metastasis. Neoplasma. 2014;61:128–35.
31. Kara M, Yumrutas O, Ozcan O, Celik OI, Bozgeyik E, Bozgeyik I, et al. Differential expressions of cancer-associated genes and their regulatory miRNAs in colorectal carcinoma. Gene. 2015;567:81–6.
32. Kara M, Kaplan M, Bozgeyik I, Ozcan O, Celik OI, Bozgeyik E, et al. MTUS1 tumor suppressor and its miRNA regulators in fibroadenoma and breast cancer. Gene. 2016;587:173–7.
33. Ranjan N, Pandey V, Panigrahi MK, Klumpp L, Naumann U, Babu PP. The tumor suppressor MTUS1/ATIP1 Modulates Tumor Promotion in Glioma: Association with epigenetics and DNA repair. Cancers (Basel). 2021;13:1245.
34. Zhao T, He Q, Liu Z, Ding X, Zhou X, Wang A, Angiotensin. II type 2 receptor-interacting protein 3a suppresses proliferation, migration and invasion in tongue squamous cell carcinoma via the extracellular signal-regulated kinase-Snai2 pathway. Oncol Lett. 2016;11:340–4.
35. Dominissini D, Moshitch-Moshkovitz S, Schwartz S, Salmon-Divon M, Ungar L, Osenberg S, et al. Topology of the human and mouse m6A RNA methylomes revealed by m6A-seq. Nature. 2012;485:201–6.
36. Niu Y, Wan A, Lin Z, Lu X, Wan G. N 6-Methyladenosine modification: a novel pharmacological target for anti-cancer drug development. Acta Pharm Sin B. 2018;8:833–43.
37. Geula S, Moshitch-Moshkovitz S, Dominissini D, Mansour AA, Kol N, Salmon-Divon M, et al. m6A mRNA methylation facilitates resolution of naive pluripotency toward differentiation. Science. 2015;347:1002–6.
38. Yang S, Wei J, Cui Y-H, Park G, Shah P, Deng Y, et al. m6A mRNA demethylase FTO regulates melanoma tumorigenicity and response to anti-PD-1 blockade. Nat Commun. 2019;10:2782.
39. Jeschke J, Collignon E, Al Wardi C, Krayem M, Bizet M, Jia Y, et al. Downregulation of the FTO m6A RNA demethylase promotes EMT-mediated progression of epithelial tumors and sensitivity to wnt inhibitors. Nat Cancer. 2021;2:611–28.
40. Wang Z, Li H, Cai H, Liang J, Jiang Y, Song F, et al. FTO sensitizes oral squamous cell carcinoma to ferroptosis via suppressing ACSL3 and GPX4. Int J Mol Sci. 2023;24:16339.
41. Li X, Xie X, Gu Y, Zhang J, Song J, Cheng X, et al. Fat mass and obesity-associated protein regulates tumorigenesis of arecoline-promoted human oral carcinoma. Cancer Med. 2021;10:6402–15.
42. Zou D, Dong L, Li C, Yin Z, Rao S, Zhou Q. The m6A eraser FTO facilitates proliferation and migration of human cervical cancer cells. Cancer Cell Int. 2019;19:321.
43. Li J, Han Y, Zhang H, Qian Z, Jia W, Gao Y, et al. The m6A demethylase FTO promotes the growth of lung cancer cells by regulating the m6A level of USP7 mRNA. Biochem Biophys Res Commun. 2019;512:479–85.
44. Shan H-J, Gu W-X, Duan G, Chen H-L. Fat mass and obesity associated (FTO)-mediated N6-methyladenosine modification of Krüppel-like factor 3 (KLF3) promotes osteosarcoma progression. Bioengineered 13:8038–50.
45. Niu Y, Lin Z, Wan A, Chen H, Liang H, Sun L, et al. RNA N6-methyladenosine demethylase FTO promotes breast tumor progression through inhibiting BNIP3. Mol Cancer. 2019;18:46.

Publisher's note

Springer Nature remains neutral with regard to jurisdictional claims in published maps and institutional affiliations.